THE JOURNAL OF BIOLOGICAL CHEMISTRY VOL. 290, NO. 14, pp. 9087–9100, April 3, 2015

HypE-specific Nanobodies as Tools to Modulate HypE-mediated Target AMPylation

Received for publication, December 30, 2014, and in revised form, February 2, 2015 Published, JBC Papers in Press, February 12, 2015, DOI 10.1074/jbc.M114.634287

Matthias C. Truttmann[‡1], **Qin Wu**[‡], **Sarah Stiegeler**[‡], **Joao N. Duarte**[‡2], **Jessica Ingram**[‡], **and Hidde L. Ploegh**[‡§3]

From the [‡]*Whitehead Institute for Biomedical Research, Cambridge, Massachusetts 02142 and the* [§]*Massachusetts Institute of Technology, Cambridge, Massachusetts 02139*

Background: Nanobodies represent a specific means to modulate enzyme function.
Results: HypE-specific nanobodies modulate AMPylation activity and identify HypE as localized to the nuclear envelope.
Conclusion: HypE function can be interfered with and probed for with new tools.
Significance: HypE nanobodies are the first known HypE activators and inhibitors.

The covalent addition of mono-AMP to target proteins (AMPylation) by Fic domain-containing proteins is a poorly understood, yet highly conserved post-translational modification. Here, we describe the generation, evaluation, and application of four HypE-specific nanobodies: three that inhibit HypE-mediated target AMPylation *in vitro* and one that acts as an activator. All heavy chain-only antibody variable domains bind HypE when expressed as GFP fusions in intact cells. We observed localization of HypE at the nuclear envelope and further identified histones H2–H4, but not H1, as novel *in vitro* targets of the human Fic protein. Its role in histone modification provides a possible link between AMPylation and regulation of gene expression.

Post-translational protein modifications represent a fundamental regulatory principle of controlling protein activities. Accordingly, modifications by proteases, kinases, methylases, or acetylases have been explored extensively, and their misregulation is often associated with severe pathology, including autoimmune diseases or cancer (1, 2). In contrast, AMPylases, which transfer an AMP moiety to a protein, are poorly understood. AMPylation, also referred to as adenylylation, was first described in the 1960s as a regulatory mechanism for controlling glutamine synthetase activity in *Escherichia coli* (1, 3). The transfer of AMP to a tyrosine residue in glutamine synthetase resulted in reversible enzyme inhibition. However, AMPylation is now known to have a role in the pathogenicity of several bacteria by translocating effector AMPylases into their host cells, where these effectors target host proteins (4–7). The bacterial effectors VopS of *Vibrio parahaemolyticus* and IbpA of *Histophilus somni* AMPylate host cell GTPases Rac1, Cdc42, and RhoA on Thr-35 and Tyr-32, respectively. The addition of a bulky AMP moiety to Thr-35 or Tyr-32 impairs binding of downstream effectors, resulting in inhibition of GTPase activity (5, 8).

Sequence comparisons and structural analysis of secreted bacterial AMPylators reveal the presence of a Fic (filamentation-induced by cAMP) domain that is essential for AMP transfer (9). All Fic domain-containing proteins (Fic proteins) share a conserved sequence motif (H*X*F*X*(D/E)GN(G/K)R). Mutation of the invariant histidine residue in VopS or IbpA abolishes their AMPylation activity (10). To regulate AMPylation, a conserved flexible α-helix (α_{inh}) containing the sequence motif (S/T)*XXX*E(G/N) is positioned to obstruct the ATP-binding site. Although, in most Fic proteins, α_{inh} is fused to the Fic domain as either an N-terminal (class II) or A C-terminal (class III) helix, α_{inh} can also exist as an independent inhibitory antitoxin (class I), as shown for the VbhT-VbhA toxin-antitoxin system (10). Substitution of the glutamic acid present in α_{inh} with glycine relieves intramolecular autoinhibition, resulting in Fic enzymes with significantly enhanced auto-AMPylation as well as enhanced target AMPylation.

Fic protein activity is not limited to the transfer of AMP onto small GTPases: the *Legionella pneumophila* Fic protein AnkX is also translocated into host cells, where it anchors a phosphorylcholine unit onto Ser-79 of Rab1 GTPases, thereby modulating host vesicle trafficking (11, 12). AvrAC from the plant pathogen *Xanthomonas campestris* covalently links UMP to RIPK and BIK1 kinases, thereby interfering with host immune defense (13). Finally, the bacterial Fic protein Doc, the toxin unit of the Doc-PhD toxin-antitoxin system present in *E. coli*, phosphorylates Thr-382 of the translation elongation factor EF-Tu, inhibiting translation (14, 15). Thus, Fic protein activity is not linked exclusively to the transfer of AMP onto target proteins. Rather, all Fic proteins share a common substrate preference (nucleoside triphosphates) for their enzymatic activities.

To date, some ~2700 Fic proteins have been identified, mostly in bacteria. Eukaryotes, including *Caenorhabditis elegans*, *Drosophila melanogaster*, *Mus musculus*, and *Homo sapiens*, encode at least one Fic protein each, with the exception of most fungi, which contain no known AMPylases (16, 17). The *Drosophila* Fic protein, referred to as CG9523 or dFic, possesses auto-AMPylation activity *in vitro*; this activity is diminished upon mutation of the conserved histidine residue within the Fic

[1] Recipient of an Early Postdoc.Mobility fellowship from the Swiss National Science Foundation.
[2] Calouste Gulbenkian Foundation Scholar. Supported by the Champalimaud Foundation, the Portuguese Science and Technology Foundation, and the Portuguese Ministry of Health.
[3] To whom correspondence should be addressed: Whitehead Inst. for Biomedical Research, 9 Cambridge Center, Cambridge, MA 02142. Tel.: 617-324-2031; Fax: 617-452-3566; E-mail: ploegh@wi.mit.edu.

motif (18). Mutant flies that lack dFic are blind, but otherwise viable. Photoreceptor cells in dFic-deficient animals depolarize normally following light stimulation, but fail to activate postsynaptic neurons, indicative of a defect in neurotransmission. Expression of enzymatically active dFic on capitate projections of glia cells, but not neurons, rescues the null phenotype. The catalytic site of dFic resides in the endoplasmic reticulum (ER)[4] lumen, where it AMPylates Thr-366 of BiP/GRP78, a conserved HSP70 family member important for quality control and regulation of the unfolded protein response in the ER (19). ER stress increases intracellular dFic and BiP levels. Conversely, AMPylation of BiP is reduced upon induction of the unfolded protein response, suggesting an inhibitory role for AMPylation in BiP activity.

The human genome encodes a single Fic protein named HypE (Huntingtin-associated yeast-interacting protein E; also referred to as FICD); it exhibits AMPylation activity against Cdc42, Rac1, and BiP *in vitro* (8). RNA expression data suggest that HypE is present in most cell types and tissues, albeit at low levels. Overexpression of wild-type HypE in cultured cells has few obvious consequences, suggesting a tight regulation of HypE activity by its inhibitory α-helix or by other, yet unidentified regulatory proteins (10). The physiological role of HypE remains elusive; however, HypE is assumed to interact with Huntingtin, a protein that, when mutated, causes Huntington disease (20), a neurodegenerative disorder.

The study of protein AMPylation in eukaryotes is limited in part by a dearth of appropriate tools to selectively track Fic proteins or modulate their activity. A threonine/AMP-specific mouse serum was used to confirm VopS-mediated AMPylation of Cdc42 and Rac1 and to study HypE-mediated BiP AMPylation (21). In addition, a set of small molecules inhibiting VopS in *in vitro* assays has been characterized (22). However, such tools are few in number. It thus remains a challenge to study the regulation and consequences of AMPylation in intact cells.

Camelid V_HHs, derived from the variable domain of heavy chain-only antibodies, present a unique tool (23, 24). V_HHs, also referred to as nanobodies, are smaller and more stable than their traditional antibody counterparts and are less dependent on disulfide bond formation for proper folding. They can therefore be expressed in the cytoplasm of bacteria (*e.g. E. coli*) or eukaryotic cells without loss of their antigen recognition properties (25). V_HHs are easily modified and can be equipped with fluorescent or affinity tags to track their target antigens within the cell (26, 27). V_HHs can serve as specific and efficient protein inhibitors or modulators and can induce changes in protein conformation within cells. Furthermore, V_HHs can stabilize transient protein conformations, facilitating protein crystallization (28).

Here, we report the generation of HypE-specific V_HHs that either inhibit or stimulate AMPylation activity *in vitro*. Three of the V_HHs inhibit histone H3 AMPylation, whereas one V_HH increases target AMPylation levels. Employing a HypE-specific mouse serum in combination with our V_HHs, we show that HypE localizes to the nuclear envelope. Finally, we identify histones H2–H4, but not H1, as new targets for HypE-promoted protein AMPylation, suggesting a possible role for HypE in regulation of gene expression or DNA repair.

[4] The abbreviations used are: ER, endoplasmic reticulum; V_HH, heavy chain-only antibody variable domain; Ni-NTA, nickel-nitrilotriacetic acid; CDR, complementarity-determining region.

EXPERIMENTAL PROCEDURES

Cell Culture

HeLa, HEK293T, and A549 cells were cultured in DMEM supplemented with 10% FBS. Transduced HeLa and A549 cell lines were cultured in DMEM supplemented with 10% FBS and G418 (Difco) at a concentration of 100 μg/ml.

Sortase-based V_HH Modification

Heptamutant Ca^{2+}-independent sortase A from *Staphylococcus aureus* ($SrtA_{staph7M}$) was purified as described (29). Sortase reaction nucleophiles GGG-TAMRA, GGG-biotin, and GGG-Alexa Fluor 647 were synthesized as described (30, 31). In-solution sortase labeling reactions with $SrtA_{staph7M}$ were performed overnight at 4 °C in 50 mM Tris-HCl (pH 7.5) and 150 mM NaCl; upon reaction completion, His_6-tagged sortase was removed from the reaction mixture using nickel-nitrilotriacetic acid (Ni-NTA) beads (Qiagen). Residual GGG nucleophiles were separated from dye-coupled V_HHs by size exclusion chromatography on PD10 columns (GE Healthcare).

Immunoblotting

Cells were seeded in 6-well plates or 10-cm^2 tissue culture dishes and transfected with Lipofectamine 2000 (Life Technologies) according to the manufacturer's instructions. After incubation for 24–48 h, cells were harvested and lysed in 50 mM Tris-HCl (pH 8.0), 150 mM NaCl, 5 mM EDTA, 1% Nonidet P-40, and 0.1% SDS supplemented with protease inhibitor mixture (Roche Applied Science). Protein samples were subjected to SDS-PAGE, transferred to a PVDF membrane, and probed with appropriate antibodies or the respective V_HH (1 μg/ml). Table 1 lists all antibodies used in this study. Chemiluminescent signals were detected using a Western Lightning ECL detection kit (PerkinElmer Life Sciences) and exposure to XAR-5 films (Kodak).

Immunofluorescence Staining

HeLa or A549 cells grown on coverslips were either transfected with respective plasmids using Lipofectamine 2000 or grown to 70–90% confluence. Cells were fixed in 4% formaldehyde and PBS for 20 min, permeabilized for 15 min in PBS and 0.3% Triton X-100, and blocked with 1% BSA and PBS. Cells were incubated for 1 h at room temperature in 1% BSA and PBS containing primary antibodies, washed three times with PBS, and incubated for another hour at room temperature in 1% BSA and PBS supplemented with Alexa Fluor 488- or Alexa Fluor 647-coupled secondary antibodies. Alternatively, cells were stained with Alexa Fluor 647-coupled V_HHs (10 μg/ml) for 1 h at room temperature. All images were collected on a PerkinElmer Ultraview multispectral spinning disk confocal microscope equipped with a Zeiss 1.4 numerical aperture oil immersion ×63 objective lens and a Prior piezoelectric objective focusing device for maintaining focus. Images were acquired with a Hamamatsu

TABLE 1
Antibodies used in this study
IF, immunofluorescence; WB, Western blotting.

Provider	Catalog no.	Specificity	Dilution used
Primary antibodies			
Sigma-Aldrich	AV46826-50UG	Human FICD	1:3000
Abcam	ab18579	GST	1:6000
Santa Cruz Biotechnology	sc-805	HA (clone Y-11)	1:500 (IF), 1:5000 (WB)
Abcam	ab16048	Lamin B1	1:100
Secondary antibodies			
Qiagen	34460	Penta-His	1:10,000
Fisher	OB4050-05	Anti-rabbit IgG (H + L)	1:25,000
SouthernBiotech	1038-05	Anti-mouse IgG (H + L)	1:25,000

ORCA ER cooled CCD camera controlled with Volocity software. Post-acquisition image manipulations were made using Fiji software. For analysis of nuclear morphology, at least 10 randomly chosen frames from three independent samples were imaged, and nuclear morphology was assessed by eye.

Coupling of V_HHs to Cyanogen Bromide-activated Beads

Beads were rinsed with 1 mM HCl for 15 min, mixed with V_HHs diluted in coupling buffer (0.1 M $NaHCO_3$ (pH 8.3) and 0.5 M NaCl), and incubated overnight at 4 °C with agitation. Beads were then washed five times with coupling buffer, blocked for 2 h at room temperature with 0.1 M Tris-HCl (pH 8.0), and subjected to at least five wash cycles with two alternating wash buffers (0.1 M acetic acid/sodium acetate (pH 4.0) and 0.5 M NaCl; and 0.1 M Tris-HCl (pH 8.0) and 0.5 M NaCl).

Competition ELISA

96-Well ELISA plates were coated with HypE or HypE E234G (0.5 μg/ml) overnight at 4 °C. Following washing and blocking with PBS, 0.1% Tween 20, and 4% milk for 2 h at 37 °C, test wells were supplemented with His-tagged unmodified V_HHs (25 μg/ml) and incubated at room temperature for 1 h. Wells were then washed and supplemented with biotinylated V_HHs (25 μg/ml), incubated at room temperature for 1 h, and analyzed using streptavidin-HRP to trigger a colorimetric readout.

Generation of Stable Cell Lines

Cell lines were engineered to allow doxycycline-inducible expression of introduced transgenes using the pINDUCER toolkit (32). Following lentiviral transduction of target cells (HeLa, A549) and subsequent selection for chromosomal integration with G418, polyclonal cell lines were assayed for GFP expression upon doxycycline addition.

Generation of HypE-specific Mouse Serum

BL52/B6 mice were subcutaneously primed with 100 μg of HypE in 100 μl of PBS supplemented with complete Freund's adjuvant, boosted by intraperitoneal injection 4 weeks later with 20 μg in PBS, and terminally bled 5 days later.

Generation of V_HHs

V_HH phage display library preparation and phage library panning were performed as described (33). Enriched V_HH sequences were cloned into a pHEN expression vector downstream of an N-terminal *pelB* sequence and equipped with a C-terminal LPTEGG sortase motif.

V_HH-HypE Interaction Tests

~50–100 μg of recombinant HypE(187–437) or HypE(187–437) E234G was incubated with 50 μg of V_HH-TAMRA at 4 °C for 2 h and analyzed on a Superdex S75 10/300 GL size exclusion column. Absorbance at 280 nm (proteins) and 545 nm (TAMRA) was recorded.

Protein Purification

HypE(187–437), HypE(187–437) E234G, and HypE(187–437) H363A—E. coli BL21(DE3) cells containing overexpression plasmids (pDuet) were grown in Terrific broth to A_{600} = 0.6, induced with 0.2 mM isopropyl β-D-thiogalactopyranoside, and incubated at 23 °C for 48 h with shaking at 200 rpm. Cells were pelleted, resuspended in lysis buffer A (50 mM Tris-HCl (pH 7.5), 150 mM NaCl, 10% glycerol, protease inhibitor mixture, and DNase I (Roche Applied Science)), and lysed with a French press. Lysate was cleared by centrifugation, and the soluble fraction was run over pre-equilibrated Ni-NTA beads. Beads were washed with 150 ml of wash buffer A (50 mM Tris-HCl (pH 7.5), 150 mM NaCl, 10% glycerol, and 10 mM imidazole) and eluted with 3 ml of elution buffer A (50 mM Tris-HCl (pH 7.5), 150 mM NaCl, 10% glycerol, and 300 mM imidazole). Ni-NTA elution fractions were further purified using a Superdex S75 16/600 column and stored in 50 mM Tris-HCl (pH 7.5), 150 mM NaCl, and 10% glycerol at 4 or −80 °C. GST-VopS was purified as described (5).

GST-HypEΔ83—E. coli BL21(DE3) cells containing overexpression plasmids were grown in LB medium to A_{600} = 0.6, induced with 0.2 mM isopropyl β-D-thiogalactopyranoside, incubated overnight at 30 °C, and purified as described (4).

His_6-Histone H3-LPTEGG—E. coli BL21(DE3) cells containing overexpression plasmids were grown in LB medium to A_{600} = 0.6, induced with 1.0 mM isopropyl β-D-thiogalactopyranoside, and incubated at 37 °C for 3 h. Cells were pelleted, resuspended in lysis buffer B (50 mM Tris-HCl (pH 7.5), 500 mM NaCl, 5% glycerol, protease inhibitor mixture, and DNase I), and lysed by sonication. Following centrifugation, the pellet was resuspended in 50 mM Tris-HCl (pH 7.5), 500 mM NaCl, 5% glycerol, and 6 M urea. The resuspended pellet was centrifuged again, and the supernatant was incubated with pre-equilibrated Ni-NTA beads for 2 h at 4 °C. Beads were washed with 150 ml of wash buffer B (50 mM Tris-HCl (pH 7.5), 500 mM NaCl, 5%

glycerol, 6 M urea, and 10 mM imidazole) and eluted with 5 ml of elution buffer B (50 mM Tris-HCl (pH 7.5), 500 mM NaCl, 5% glycerol, 6 M urea, and 250 mM imidazole). Eluted histones were dialyzed overnight against 50 mM Tris-HCl (pH 7.5), 150 mM NaCl, and 10% glycerol and stored at 4 or −80 °C.

V_HHs—1 liter of LB medium was inoculated overnight with a 10-ml culture of *E. coli* WK6 containing V_HH-encoding pHEN6 plasmids. Protein expression was induced at $A_{600} = 0.6$ with 1.0 mM isopropyl β-D-thiogalactopyranoside, and bacteria were grown overnight at 30 °C. The following day, bacteria were pelleted, resuspended in 20 ml of 1× TES (0.2 M Tris-HCl (pH 8.0), 0.65 mM EDTA, and 0.5 M sucrose), and incubated at 4 °C for 1 h. Bacteria were then repelleted, resuspended in 60 ml of 0.25× TES, and incubated overnight at 4 °C. Following centrifugation for 30 min at 10,000 × *g*, the supernatant was incubated with pre-equilibrated Ni-NTA at 4 °C for 1 h. Beads were transferred into a gravity flow column, washed with 150 ml of wash buffer A, and eluted with 3 ml of elution buffer A. Elution fractions were further purified on a Superdex S75 16/600 column and stored at −80 °C.

In Vitro AMPylation Assays

5–10 μg of HypE(187–437), HypE(187–437) E234G, or HypE(187–437) H363A in 10 μl were first mixed with 25 μl of 50 mM Tris-HCl (pH 7.5), 150 mM NaCl, 7.5 mM $MgCl_2$, and 0.1 mM DTT supplemented with 0.5 μCi of [α-^{33}P]ATP. The reaction was allowed to proceed for 1 h at room temperature, followed by the addition of 1–5 μg of target protein (histones) in a 10-μl volume. The reaction mixture was incubated for another hour at room temperature, supplemented with 10 μl of reducing SDS sample buffer, boiled for 5 min, and analyzed on 10–15% SDS-polyacrylamide gels. For V_HH inhibition assays, HypE(187–437) proteins were incubated with the respective V_HHs for 1 h at room temperature prior to the addition of [α-^{33}P]ATP-containing reaction buffer. Human histones H1, H2A, H2B, H3.1, H3.2, H3.3, and H4 were purchased from Sigma. Autoradiograph signal intensities were analyzed using the gel analysis macro included in the Fiji software package (34).

Cell Viability Assays and FACS Analysis

Cells were grown in 12-well plates, transfected with the indicated plasmids, and incubated for 36 h. Cells were then trypsinized and treated with LIVE/DEAD fixable violet dead cell stain (Life Technologies) according to the manufacturer's instructions. Data acquisition was performed with a BD LSR II system (BD Biosciences) using CellQuest Pro software (BD Biosciences). Data were analyzed with FlowJo (Tree Star Inc.).

RESULTS

Characterization of HypE-specific V_HHs—Camelid-derived V_HHs are potent and specific tools for studying protein function (35). To generate HypE-specific V_HHs, we immunized an alpaca with HypE(187–437) E234G, harvested its peripheral blood lymphocytes, and used V_HHs amplified from this sample to generate a V_HH phagemid library. Fig. 1*A* provides a schematic overview of the process. Phage display was then performed using immobilized HypE(187–437) or HypE(187–437) E234G as the bait protein. Sequencing of 192 individual V_HH clones isolated after two subsequent rounds of panning revealed 17 clones present at least twice in the collection, with the most abundant clone recovered from six independent colonies. We subcloned 10 unique V_HH sequences into a pHEN6 periplasmic expression vector and installed a C-terminal LPETGG-His_6 tag to facilitate protein purification and render the V_HH a substrate for a sortase-based transpeptidation reaction. All candidates were expressed with yields varying from 2 to 40 mg/liter of *E. coli* culture. To assay the specificity of the V_HHs for HypE, we first tested the V_HHs in immunoblots using the V_HH as a primary antibody at a concentration of 1 μg/ml (Fig. 1*B*). Four of 10 V_HHs detected GST-HypEΔ83 and showed no reactivity toward GST-VopS, indicating their specificity (Fig. 1*C*). Sequence alignment of the V_HHs showed that, as expected, most sequence heterogeneity is found in the complementarity-determining regions (CDRs), particularly in CDR3 (Fig. 1*D*). Although V_HH-8 and V_HH-1 represent the most similar V_HH pair, V_HH-9 is the most distant representative based on sequence homology analysis (26).

In the next step, we covalently linked a TAMRA moiety to the C terminus of our HypE-specific V_HHs by sortagging, resulting in site-specifically, fluorescently labeled V_HHs. These modified V_HHs were then incubated with recombinant HypE(187–437) E234G at 1:1 molar ratio, and complex formation was analyzed by size exclusion chromatography (Fig. 2, *A* and *B*). We observed stable complex formation of HypE(187–437) E234G with V_HH-8, V_HH-1, and V_HH-2 and of HypE(187–437) with V_HH-100, as inferred from 1) a slight left shift in the HypE(187–437) E234G-corresponding elution peak (~10.5 ml), 2) the disappearance of the V_HH-TAMRA elution peak (~14 ml), and 3) the shift in the TAMRA signal from the V_HH elution peak to the HypE elution peak. In contrast, V_HH-9 failed to form a complex with native HypE(187–437) E234G. To corroborate these results, we coupled four V_HHs to CNBr-activated beads, immunoprecipitated HypE from HeLa cell lysates, and probed the precipitated fractions with a commercial anti-HypE polyclonal antibody. As indicated in Fig. 2*C*, beads coupled with V_HH-1, V_HH-2, and V_HH-8, but not V_HH-9, recovered HypE from cell lysates, albeit with different efficiencies. Furthermore, competition ELISAs showed that V_HH-8 and V_HH-1 competed for binding on HypE(187–437) E234G, suggesting that they recognize overlapping epitopes (Fig. 2*D*).

V_HHs Inhibit or Stimulate HypE-mediated Target AMPylation in Vitro—The Fic domain of HypE has been associated with AMPylation activity both *in vitro* and *in vivo* (19). To test if our V_HHs interfere with auto-AMPylation and target AMPylation, we incubated recombinant HypE(187–437) E234G with excess V_HH for 1 h before supplementing the reaction with [α-^{33}P]ATP and recombinant human histone H3 as a substrate. The purity of the recombinant histone H3 preparation used in these assays is depicted in Fig. 3*A*, which shows the presence of some remaining contaminating polypeptides. V_HH-8, V_HH-1, and V_HH-2 interfered with auto-AMPylation and target AMPylation to different extents (Fig. 3*B*). In contrast, V_HH-9 and V_HH-100 had no detectable effect on HypE(187–437) E234G target AMPylation, although V_HH-100 decreased the auto-AMPylation activity of HypE(187–437) E234G (Fig. 3, *B* and *C*). Titration experiments showed a dose dependence of

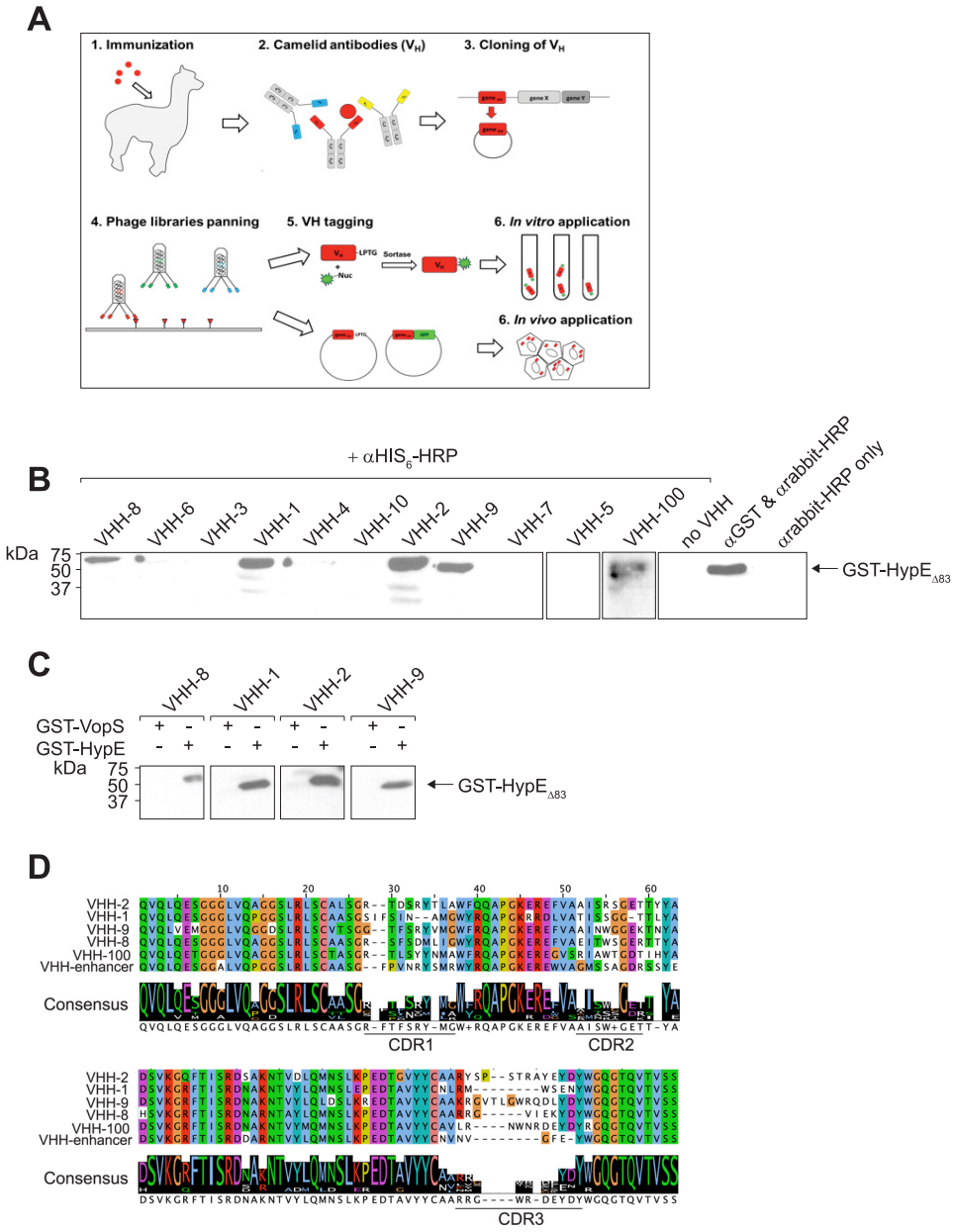

FIGURE 1. **Initial characterization of HypE-specific V_HHs by immunoblotting and overview of the generation of V_HHs.** *A*, schematic representation of V_HH generation. *B*, an initial test of 10 putative HypE-specific V_HHs in immunoblot assays. His_6-V_HHs were probed against GST-HypEΔ83 and detected using an anti-His_6-HRP antibody. *C*, evaluation of cross-reactivity of V_HHs binding to GST-HypEΔ83. His_6-tagged V_HHs were probed against GST-HypEΔ83 and GST-VopS and detected using an anti-His_6-HRP antibody. *D*, sequence alignment of characterized anti-HypE V_HHs, including an anti-GFP V_HH (enhancer) as reference. CDR1–CDR3 are *underlined*.

HypE(187–437) E234G inhibition, with V_HH-1 emerging as the most potent, with almost complete inhibition at a 5:1 molar ratio of V_HH to HypE(187–437) E234G (Fig. 3*D*). Notably, complex formation between HypE(187–437) and V_HH-100 enhanced auto-AMPylation and target-AMPylation by HypE-(187–437) (Fig. 3*E*), whereas V_HH-1, V_HH-2, and V_HH-8 did not (data not shown). The V_HHs described here represent the first examples of HypE-specific AMPylation inhibitors or enhancers.

Endogenous HypE Is Localized to the Nuclear Envelope—To complement our V_HH-based approach with another HypE-specific tool, we generated a HypE-specific mouse serum, as commercially available sera had proved inadequate. This serum efficiently detected HA-tagged HypE constructs overexpressed in HeLa cells (Fig. 4*A*). We co-stained HeLa cells overexpressing HA-HypE with anti-HypE serum and an anti-HA antibody. We observed co-localization of both labels, demonstrating the serum's specificity for HypE and its utility in immunofluorescence (Fig. 4*B*). In cells that overexpress HypE, the protein was present in the nuclear envelope and associated structures. The latter likely represent the endoplasmic reticulum. To confirm the intracellular localization of HypE, we stained untransfected HeLa cells with anti-HypE serum and co-labeled the cells with an anti-lamin AC antibody. The majority of endogenous HypE resides in the nuclear lamina, as indicated by the extensive co-localization of HypE and the lamina-specific signal (Fig. 4*C*).

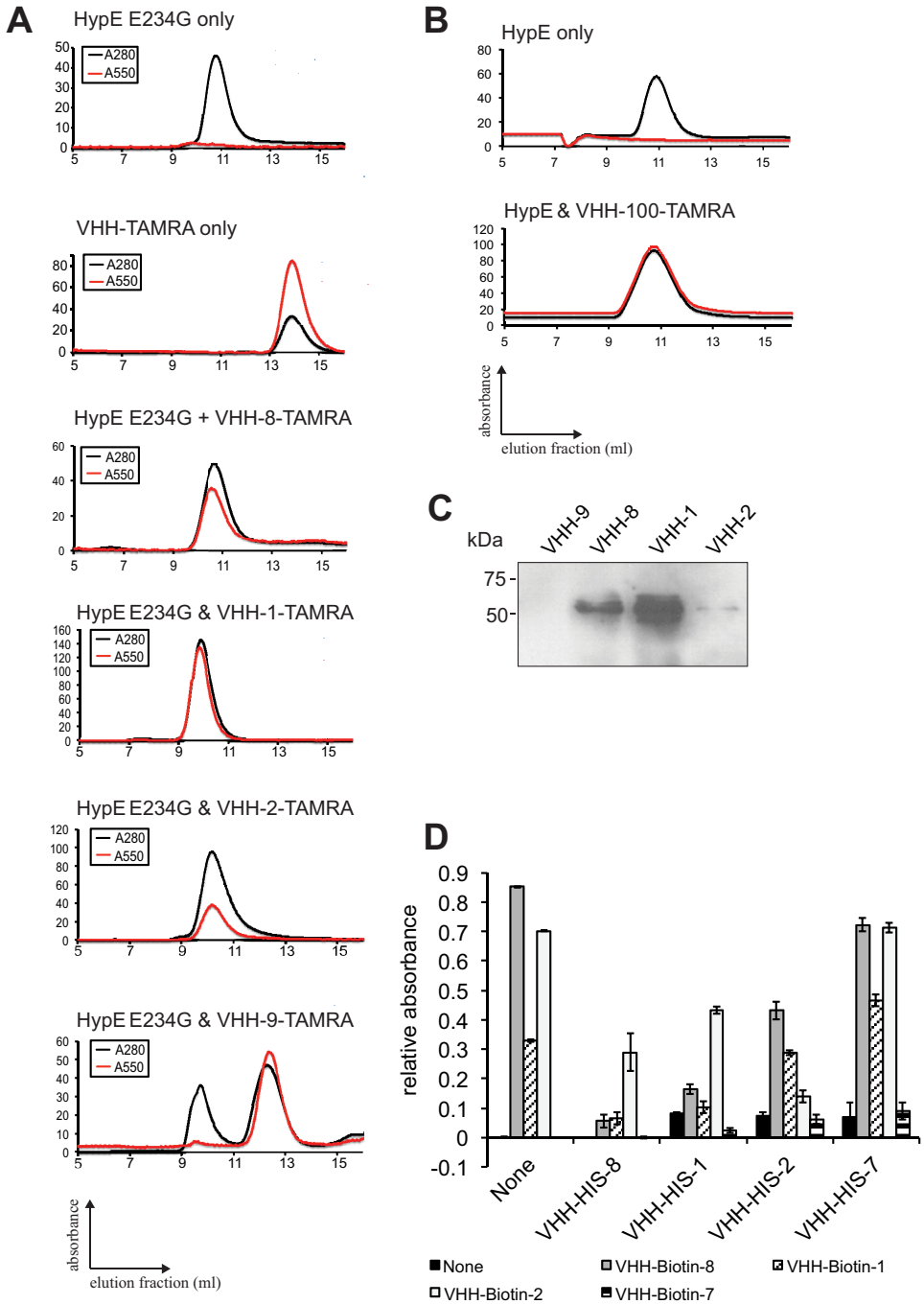

FIGURE 2. **Validation and characterization of HypE-specific V_HHs.** Recombinant HypE(187–437) E234G (*A*) and HypE(187–437) (*B*) were incubated with TAMRA-labeled V_HHs. Complex formation was assessed by size exclusion chromatography. *Black lines* (A_{280}) represent total protein, and *red lines* (A_{545}) represent the TAMRA signal. *C*, endogenous HypE was immunoprecipitated from HeLa cell lysates using V_HH-coupled beads and analyzed by Western blotting with a commercial anti-HypE antibody. *D*, competition ELISAs were performed using His_6-V_HHs for initial epitope masking and biotin-V_HH for subsequent probing.

V_HHs Recognize HypE in Live and Fixed Cells—To determine whether our V_HHs interact with HypE in an intact cellular environment, we generated HeLa cell lines that contain an inducible GFP-V_HH expression cassette for the anti-HypE V_HHs. Upon induction with doxycycline, GFP-V_HHs were distributed throughout the cell, including the nucleus (Fig. 5, *A–C*, and Fig. 6, *A* and *B*). Ectopic expression of HA-tagged HypE constructs in cells that express GFP-V_HH-8, GFP-V_HH-1, GFP-V_HH-2, and GFP-V_HH-100 resulted in robust co-localization of the V_HHs with HA-HypE, whereas the GFP signal remained diffuse in cells expressing GFP-V_HH-9. To further test our V_HHs, we engineered V_HH-Alexa Fluor 647 fusions by sortagging (29) and used these to stain fixed HypE-overexpressing cells (Fig. 7, *A* and *B*). As with the GFP-tagged V_HHs, we observed robust co-localization of our V_HHs with HA-HypE, establishing that directly labeled V_HHs are useful tools for microscopy.

HypE AMPylates Histones H2–H4, but Not H1—To explore the role of HypE in intact cells, we set out to identify novel HypE

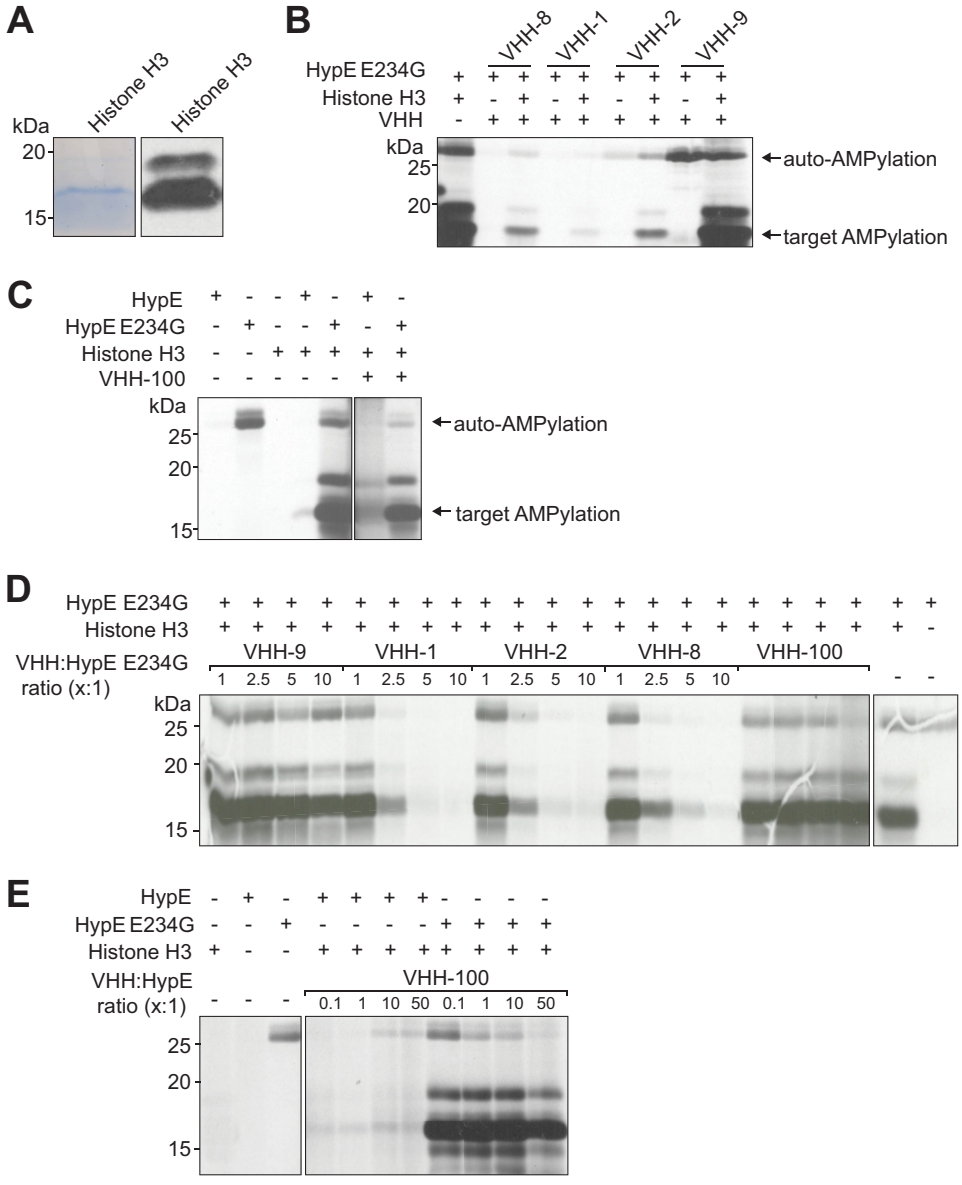

FIGURE 3. **V_HHs modulate HypE E234G-mediated target AMPylation.** *A*, recombinant histone H3 was separated by SDS-PAGE and either visualized by Coomassie Brilliant Blue staining (*left panel*) or transferred to a PVDF membrane and probed with an anti-His_6-HRP antibody (*right panel*). Recombinant HypE(187–437) E234G (*B*) or HypE(187–437) (*C*) was incubated with an excess of the respective V_HHs for 1 h at room temperature, at which point [α-^{33}P]ATP and histone H3 substrate were added, and the mixture was incubated for an additional hour. Incorporation of label was assessed by SDS-PAGE and autoradiography. *D*, dose dependence of V_HH-mediated HypE inhibition. Recombinant HypE(187–437) E234G was incubated with the respective V_HHs at the indicated ratios for 1 h at room temperature, combined with [α-^{33}P]ATP and histone H3 substrate, and incubated for another hour. Sample autoradiography was assessed. *E*, dose dependence of V_HH-mediated HypE activation. Recombinant HypE(187–437) or HypE(187–437) E234G was incubated with the respective V_HHs at the indicated ratios for 1 h at room temperature, combined with [α-^{33}P]ATP and histone H3 substrate, and incubated for another hour. Sample autoradiography was assessed.

target proteins. As endogenous HypE localized to the nuclear envelope, we focused on nucleus-associated proteins, including histones. Histone H3 has been reported to be a substrate for HypE (22). We systematically tested representatives of all major histone classes (H1, H2A, H2B, H3.1, H3.2, H3.3, and H4) in *in vitro* AMPylation assays and observed that HypE(187–437) and HypE(187–437) E234G AMPylated histones H2A, H2B, H3.1, H3.2, H3.3, and H4, but not H1 (Fig. 8, *A* and *B*). Comparing the signal intensities observed for HypE(187–437)- and HypE(187–437) E234G-mediated histone H3 AMPylation, we calculated that HypE E234G showed an ~30-fold increase in AMPylation activity compared with the wild-type enzyme. Unbiased motif identification using MEME with histones H2–H4 as positive input and histone H1 as negative input did not suggest the obvious presence of a conserved motif for AMPylation (36). However, as HypE has been associated with tyrosine AMPylation of small GTPases, we constructed and purified a set of mutant histone H3 constructs in which we exchanged all tyrosines for phenylalanines or retained a single tyrosine. *In vitro* AMPylation tests using these histone H3 mutants demonstrated that even the tyrosine-free version was still AMPylated by HypE E234G (Fig. 8*C*). However, we observed significantly decreased AMPylation levels for tyrosine-free histone H3, whereas the reduction in AMPylation

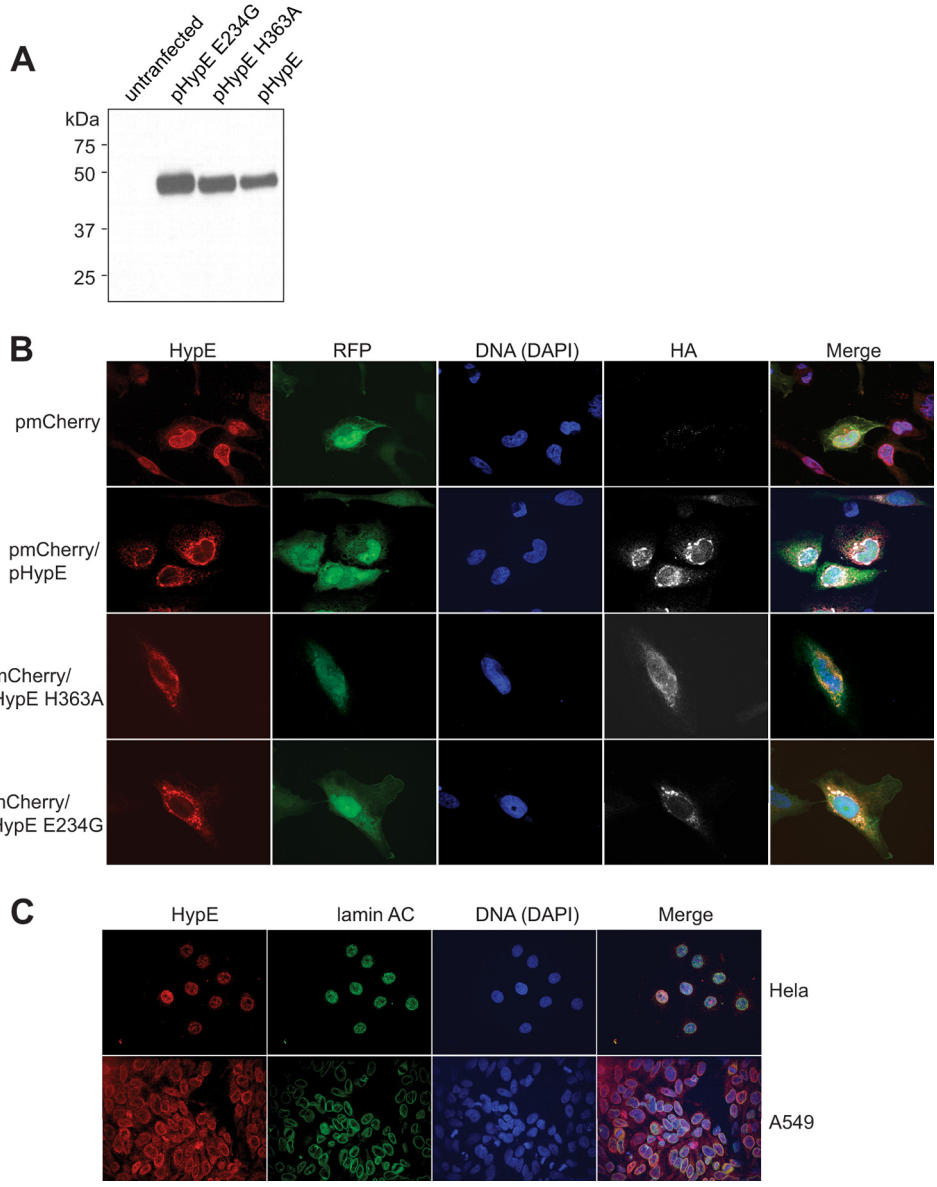

FIGURE 4. **Characterization of HypE-specific mouse serum.** *A*, cell lysates of pHypE-, pHypE E234G-, or pHypE H363A-transfected cells were probed with HypE-specific serum. *B*, co-staining of fixed HeLa or A549 cells with HypE-specific serum, anti-lamin antibody, and DAPI (DNA). *C*, co-staining of pHypE-, pHypE E234G-, or pHypE H363A-transfected HeLa cells with HypE-specific serum, anti-HA antibody, and DAPI (DNA).

observed for single tyrosine-containing histones was less pronounced (Fig. 8*D*). The fact that even the tyrosine-free histone version was AMPylated indicates at least one non-tyrosine site of AMPylation, likely Ser, Thr, or His. Time course experiments in which we compared the AMPylation of wild-type *versus* tyrosine-free histone H3 showed similar kinetics, although wild-type histone H3 was AMPylated at a significantly higher level (Fig. 9, *A* and *B*) compared with the tyrosine-free variant.

Intracellular Hyper-AMPylation by HypE E234G Intoxicates Cells—In the course of our experiments, we noticed that cells ectopically expressing the hyperactive mutant HypE E234G showed obvious signs of cellular stress and increased cell death rates. To quantify these findings, we co-transfected HeLa cells with mCherry and pHypE constructs and assayed for cell death. Transfected cells were selected for analysis based on the presence of the mCherry signal. Overexpression of HypE E234G was toxic and significantly increased cell death (Fig. 9*C*). Furthermore, populations of cells that expressed HypE E234G displayed an increased number of cells with misshapen nuclei (Fig. 9*D*). The abnormal nuclei were of approximately the same size as regular nuclei, but were severely misshapen and often showed signs of a ruptured envelope or nuclear bleb-like structures (Fig. 9*E*), in contrast to apoptotic nuclei, which are characterized by DNA condensation and an increase in DNA staining intensity. Cells overexpressing either HypE or the active-site mutant HypE H363A showed neither increased death rates nor any signs of aberrant nuclear morphology, indicating that the observed changes are linked to increased AMPylation by HypE E234G. The HypE substrate(s) responsible for imposition of altered nuclear morphology remain to be identified.

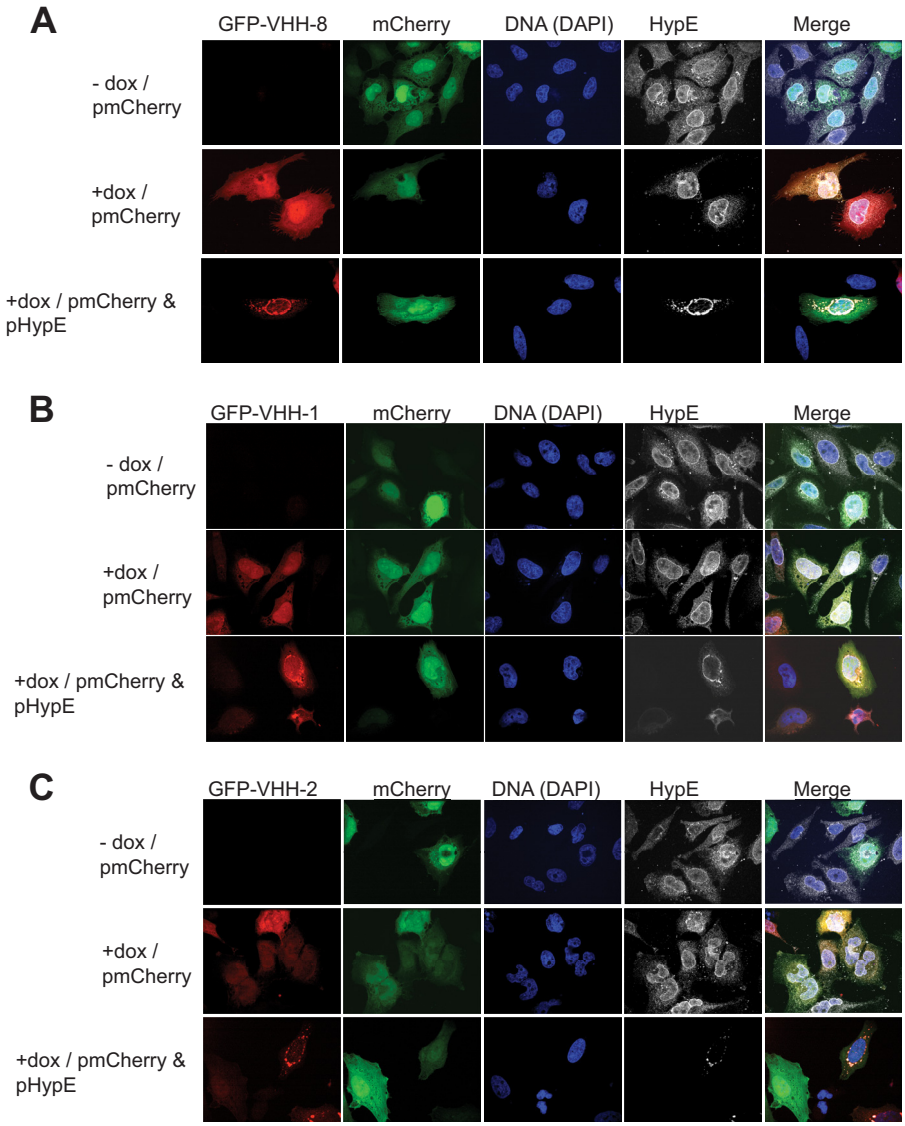

FIGURE 5. **GFP-tagged V_HHs bind to HypE in intact cells.** pmCherry- or pmCherry/pHypE-transfected HeLa cells inducibly expressing GFP-tagged V_HH-8 (*A*), V_HH-1 (*B*), or V_HH-2 (*C*) were stained with HypE-specific mouse serum. *dox*, doxycycline.

DISCUSSION

Target AMPylation by Fic domain-containing enzymes represents a conserved protein modification mechanism. Although translocated bacterial Fic proteins perturb host cell signaling during infections, the *D. melanogaster* Fic protein, dFic, resides within the ER lumen, where it AMPylates BiP, an essential ER chaperone involved in regulation of the unfolded protein response (5, 19). However, despite the fact that the human Fic protein HypE was shown to AMPylate Cdc42, Rac1, and BiP in *in vitro* assays, the localization of HypE, its physiologically most relevant targets, and its role in regulating cell signaling mechanisms remain elusive.

This work describes camelid-derived V_HHs specific for HypE that allow an examination of HypE localization and function. We established the specificity of the V_HHs for HypE and demonstrated their versatility in the several applications reported here. The anti-HypE V_HHs allowed us to specifically manipulate HypE function *in vitro*. We used a sortase-based approach to generate Alexa Fluor 647-, TAMRA-, and biotin-modified anti-HypE V_HHs, demonstrating that their C-terminal modification does not impair function. The requirements for proper disulfide bond formation and glycosylation confound intracellular expression of full-sized antibodies and most antibody fragments in the reducing environment of the cytoplasm (37). V_HHs can function without these modifications (25). The HypE-specific V_HHs are efficiently expressed in HeLa cells fused at their C terminus to GFP. Co-localization of GFP-tagged V_HHs in HeLa cells with ectopically expressed HypE constructs indicates that the GFP tag does not interfere with the ability of a V_HH to bind to its designated target protein. Although our anti-HypE polyclonal serum readily detected endogenous HypE levels, our V_HH-Alexa Fluor 647 fusions performed less well because the signal intensity of sortase-labeled V_HHs is limited to a single fluorophore.

From the set of GFP-tagged V_HHs, only V_HH-8-GFP showed occasional co-localization with the nuclear envelope in untransfected cells. Endogenous HypE levels were low, and therefore, the more highly expressed V_HH-GFP fusions

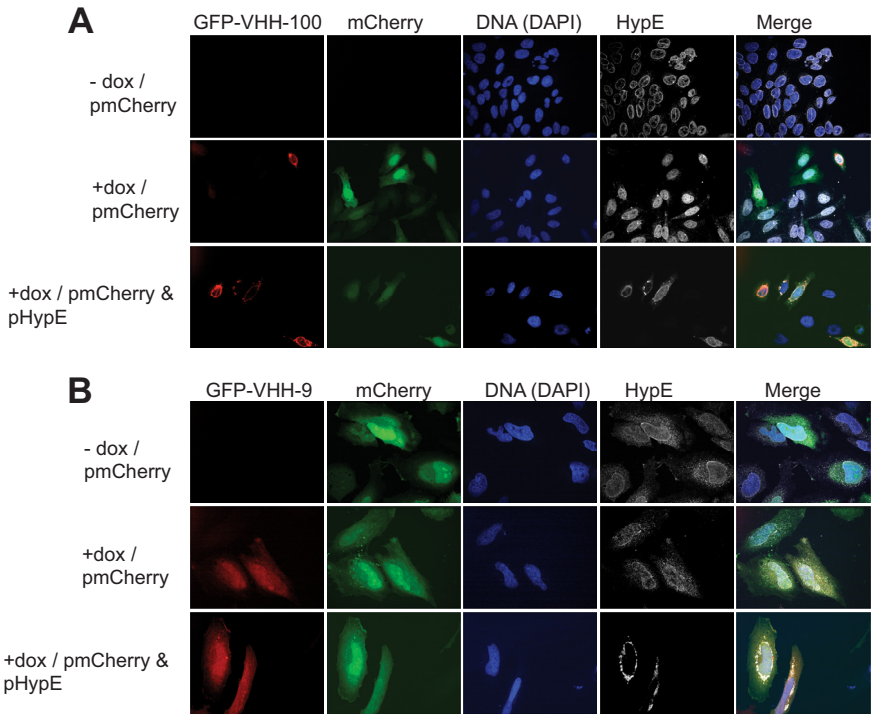

FIGURE 6. **GFP-tagged V_HHs bind to HypE in intact cells.** pmCherry- or pmCherry/pHypE-transfected HeLa cells inducibly expressing GFP-tagged V_HH-100 (*A*) or V_HH-9 (*B*) were stained with HypE-specific mouse serum. *dox*, doxycycline.

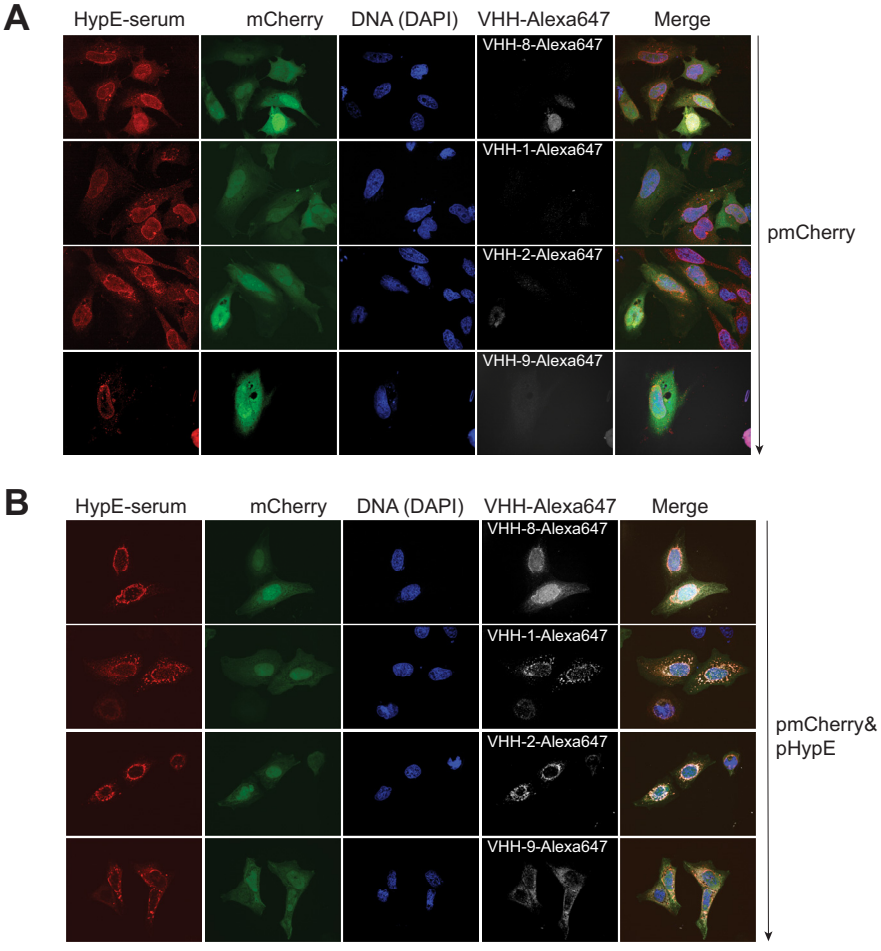

FIGURE 7. **Alexa Fluor 647-linked V_HHs recognize HypE in fixed cells.** pmCherry-transfected (*A*) or pmCherry/pHypE-transfected (*B*) cells were stained with HypE-specific mouse serum and Alexa Fluor 647-coupled V_HHs.

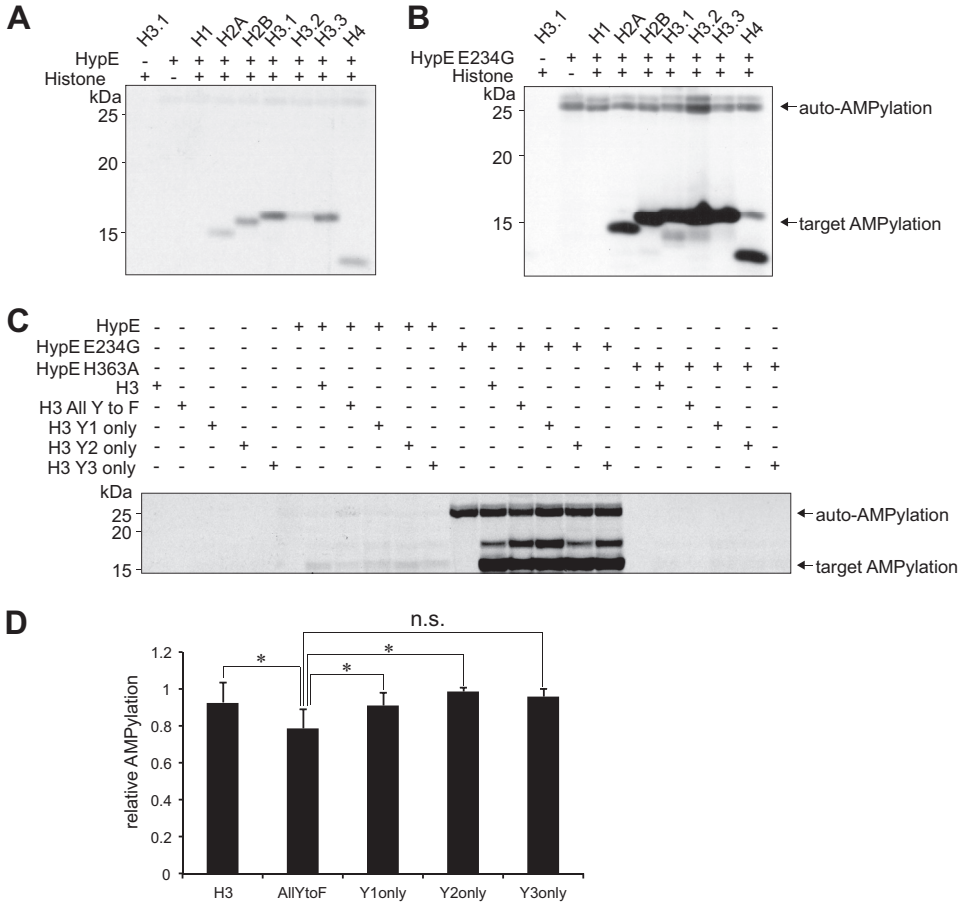

FIGURE 8. **HypE AMPylates histones H2A–H4, but not H1.** Recombinant HypE(187–437) (*A*) and HypE(187–437) E234G (*B*) were incubated with [α-^{33}P]ATP for 1 h and mixed with the respective histone substrates for another hour. Incorporation of label was assessed by SDS-PAGE and autoradiography. *C*, recombinant HypE(187–437), HypE(187–437) E234G, and HypE(187–437) H363A were incubated with [α-^{33}P]ATP for 1 h and mixed with the respective histone mutant substrates for another hour. Incorporation of label was assessed by SDS-PAGE and autoradiography. *D*, quantification of histone mutant AMPylation by HypE(187–437) E234G. The average of three independent experiments is shown. *, $p < 0.05$. *AllYtoF*, all tyrosines substituted with phenylalanines; *Y1only*, *Y2only*, and *Y3only*, only a single tyrosine retained; *n.s.*, not significant.

remained free and dispersed throughout the cell, masking those few V_HH-GFP molecules that interacted with HypE at the nuclear envelope.

The V_HHs identified in this study represent the first HypE-specific inhibitors or enhancers with demonstrated *in vitro* activity. A recent study characterized small molecule inhibitors of VopS; however, these molecules failed to rescue VopS-induced cell rounding and subsequent cell death in tissue culture assays (22). There are other examples of inhibiting or neutralizing V_HHs (35), but only a few V_HHs have shown stimulatory activity, such as a pair of V_HHs capable of increasing the zymogen activity of the carboxypeptidase TAFI (38). The HypE-specific V_HHs remain functional when expressed in HeLa cells, as indicated by co-localization with HypE. As we still do not understand how endogenous HypE regulates cellular processes and the consequences of its inhibition, we cannot at present provide functional data that confirm the inhibitory or stimulatory activity of a V_HH when expressed inside cells. Because the HypE-binding sites of the individual V_HHs remain to be mapped, we can only speculate how these V_HHs inhibit or stimulate AMPylation. Enzyme inhibition most likely arises from steric interference with or occlusion of the active site, avoiding proper nucleotide turnover and target binding. Stimulation of auto-AMPylation and AMP transfer may result from V_HHs stabilizing an enzyme confirmation that resembles the mutant E234G state, with presumably more direct access to the active site. Recent structural work on HypE and HypE E234G suggested that HypE dimerizes in a Fic domain-dependent fashion. Mutation of Leu-258 abolishes HypE dimerization and greatly reduces auto-AMPylation (39). Other mutations in the dimerization interface inhibit HypE auto-AMPylation without fully blocking dimerization. Thus, our inhibitory HypE V_HHs might occlude the dimerization interface and phenocopy the Leu-258 mutation. Solving the structure of a V_HH-HypE co-crystal is likely to clarify the mechanism of action of the individual V_HHs. The ability of V_HHs to serve as crystallization chaperones will be a useful attribute in this regard (33).

We found that human HypE localizes to the nuclear envelope, in contrast to the ER lumenal localization reported for the *Drosophila* Fic protein dFic. Furthermore, recent work by Sanyal *et al.* (40) suggested that HypE may not only localize to the ER, but may also be present in the nuclear envelope, as evident from immunofluorescence images. The inner and outer nuclear membranes are contiguous with the endoplasmic reticulum, and certain proteins have been shown to freely diffuse between the two cellular compartments, as HypE may (41). We found

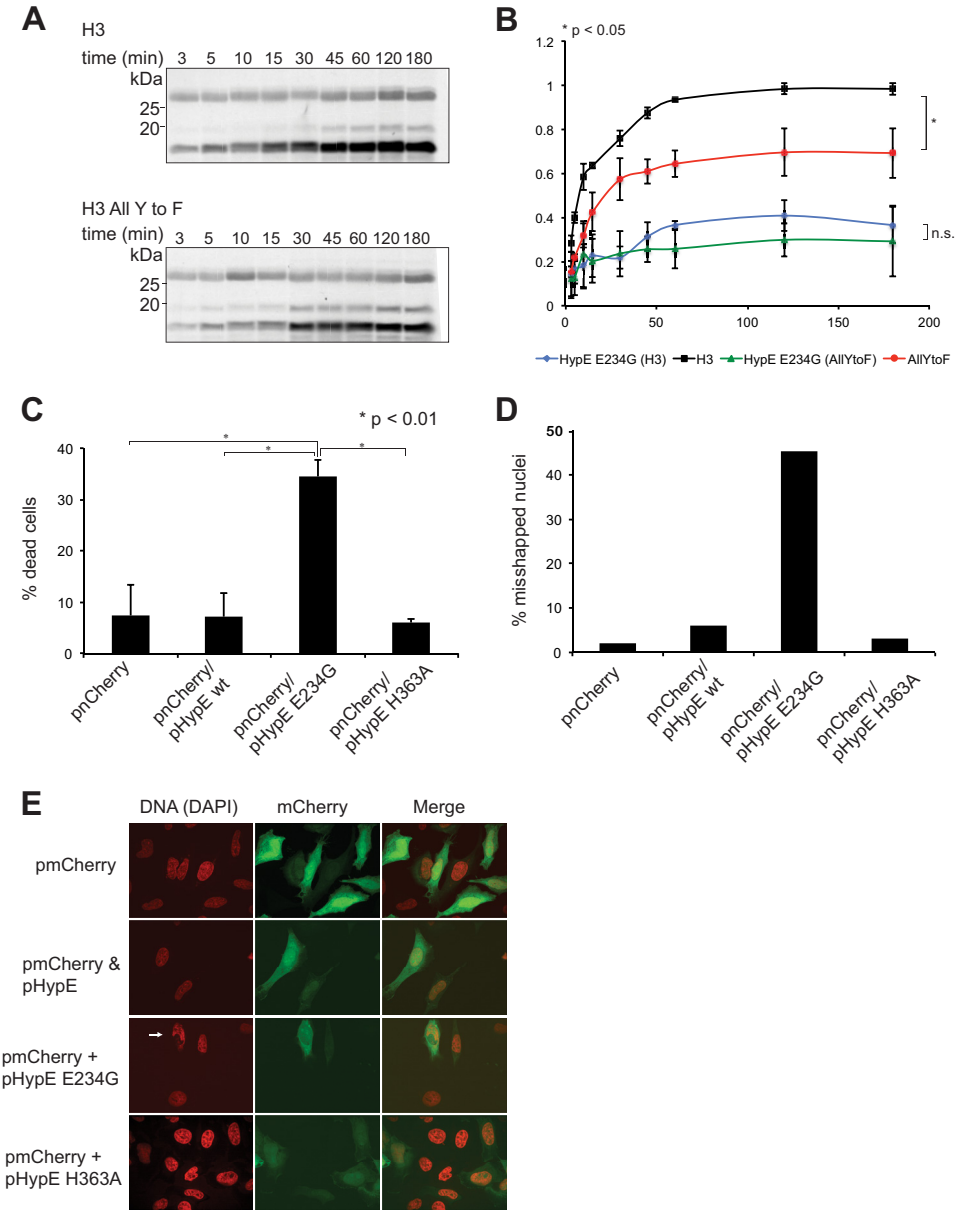

FIGURE 9. **HypE E234G AMPylates tyrosine-free histone H3 and induces cell death.** Shown are the kinetics of HypE(187–437) E234G-mediated histone H3 and tyrosine-free histone H3 mutant AMPylation. A representative autoradiogram is depicted in *A*, and the quantification of histone AMPylation by HypE(187–437) E234G is shown in *B* (average of three independent experiments). *, $p < 0.05$. *All Y to F*, all tyrosines substituted with phenylalanines; *n.s.*, not significant. *C*, A549 cells were transfected with the indicated plasmids, incubated for 48 h, stained with a vital dye, and analyzed by FACS. The average of three independent experiments is shown. *D*, distribution of misshaped nuclei in transfected HeLa cells. Collective data obtained from analysis of at least 10 frames from three independent samples are shown. *E*, staining of HeLa cells transfected with indicated plasmids for 48 h. The *arrow* indicates a typical abnormal nucleus in a HypE E234G-expressing cell.

that especially in cells overexpressing HypE, the protein not only localizes to the nuclear membrane, but also is seen in other compartments in the perinuclear space that are likely to represent the ER, possibly as a consequence of overexpression.

The mechanism that underlies the aberrant nuclear morphology observed in response to overexpression of HypE E234G remains to be identified. Neither HypE nor HypE H363A overexpression affects nuclear morphology. Rather, aberrant nuclear shape appears to be linked to the AMPylation activity of HypE. Similar nuclear blebbing is seen in fibroblasts derived from major lamin A-only knock-out mice (42). However, these aberrations are not linked to any obvious decrease in fitness. Thus, we assume that the changes in nuclear morphology do not account for increased cell death seen in cells that overexpress HypE E234G.

The localization of endogenous HypE suggests a possible role for this enzyme in genome-associated processes. Interestingly, most bacterial Fic proteins contain a DNA-binding domain such as a helix-turn-helix motif, suggesting a possible link between Fic protein activity and DNA biology.

Histone modifications by methylases, acetylases, and other enzymes regulate gene expression in eukaryotes. We identified histones H2A, H2B, H3.1, H3.2, H3.3, and H4, but not H1, as *in vitro* substrates for the human Fic protein HypE. The N-terminal histone tail extensions protrude from the nucleosome and are targeted by methylases and additional modifying enzymes. Histone H1 is not part of the nucleosome; instead, it stabilizes chromatin structure by binding DNA between individual nucleosome core particles. Histone H1 is the most variable his-

tone across species, and N-terminal modifications are less prevalent. Histone modifications are not limited to small covalent additions such as methylation or phosphorylation: all core histones (H2–H4) as well as the linker histone H1 (43) can undergo poly(ADP-ribosylation). Histone poly(ADP-ribosylation) is most pronounced following genotoxic stress inducing DNA strand breaks (44). However, detection of histone poly(ADP-ribosylation) is complicated by the fact that only a small fraction of histones are modified, as may be the case for AMPylation as well.

Our *in vitro* AMPylation results demonstrate that histone AMPylation is not restricted to tyrosines, as a tyrosine-free mutant was still readily modified by HypE E234G. The use of [α-^{33}P]ATP ensured that we were monitoring AMPylation, as distinct from phosphorylation. Furthermore, a mutant version of histone H3 containing phenylalanines instead of tyrosines was AMPylated less well than wild-type histone H3. Whether this reduction in AMPylation is indicative of tyrosine AMPylation or rather the consequence of altered folding remains to be tested.

The list of HypE substrates has been extended recently by the addition of BiP, an ER-located HSP70 family member (19, 40). BiP is modified on Ser-365 and Thr-366, suggesting that HypE is capable of AMPylation of serine, tyrosine, and threonine residues. Threonines are far more prevalent in histones and are obvious kinase targets such as Chk1 (45). How histone AMPylation relates to other modifications such as methylation, acetylation, ubiquitylation, and phosphorylation remains to be investigated. Despite considerable efforts, we have not been able to localize the precise site(s) of histone AMPylation by MS. Proteolytic digests of histone H3 with commonly used proteases result in very small peptides difficult to retain, ionize, and detect by MS (46), reflected also by the poor sequence coverage we observed in our MS experiments (data not shown). In addition, MS analysis of intact *in vitro* AMPylated histone H3 indicated that only a small fraction (<1%) of the input protein was modified, as reported for histone ADP-ribosylation, thus further complicating the detection of AMPylated histone H3-derived peptides by MS (data not shown).

We have described HypE-specific V_HHs that inhibit or enhance HypE-promoted auto-AMPylation and target AMPylation. In addition, we have localized HypE to the nuclear envelope and established that histones H2–H4, but not H1, are novel HypE targets. Consequently, HypE might be involved in the regulation of gene expression, DNA repair, or other histone-associated processes in human cells. Whether histone AMPylation may prove to be an epigenetic mark will require more extensive genetic and biochemical analysis.

Acknowledgments—We are grateful to the members of the Ploegh laboratory for stimulating discussions and suggestions. Denise Alwing and Marie-Lyne Tatlock are acknowledged for technical assistance with protein purification. We thank Wendy Salmon (Keck imaging facility) for confocal imaging assistance and the Whitehead FACS facility for help with FACS-based assays. Finally, we acknowledge Christoph Dehio for providing HypE-encoding plasmids.

REFERENCES

1. Brown, M. S., Segal, A., and Stadtman, E. R. (1971) Modulation of glutamine synthetase adenylylation and deadenylylation is mediated by metabolic transformation of the PII regulatory protein. *Proc. Natl. Acad. Sci. U.S.A.* **68,** 2949–2953
2. O'Shea, J. J., Holland, S. M., and Staudt, L. M. (2013) JAKs and STATs in immunity, immunodeficiency, and cancer. *N. Engl. J. Med.* **368,** 161–170
3. Chock, P. B., Rhee, S. G., and Stadtman, E. R. (1980) Interconvertible enzyme cascades in cellular regulation. *Annu. Rev. Biochem.* **49,** 813–843
4. Mattoo, S., Durrant, E., Chen, M. J., Xiao, J., Lazar, C. S., Manning, G., Dixon, J. E., and Worby, C. A. (2011) Comparative analysis of *Histophilus somni* immunoglobulin-binding protein A (IbpA) with other Fic domain-containing enzymes reveals differences in substrate and nucleotide specificities. *J. Biol. Chem.* **286,** 32834–32842
5. Yarbrough, M. L., Li, Y., Kinch, L. N., Grishin, N. V., Ball, H. L., and Orth, K. (2009) AMPylation of Rho GTPases by *Vibrio* VopS disrupts effector binding and downstream signaling. *Science* **323,** 269–272
6. Palanivelu, D. V., Goepfert, A., Meury, M., Guye, P., Dehio, C., and Schirmer, T. (2011) Fic domain-catalyzed adenylylation: insight provided by the structural analysis of the type IV secretion system effector BepA. *Protein Sci.* **20,** 492–499
7. Xiao, J., Worby, C. A., Mattoo, S., Sankaran, B., and Dixon, J. E. (2010) Structural basis of Fic-mediated adenylylation. *Nat. Struct. Mol. Biol.* **17,** 1004–1010
8. Worby, C. A., Mattoo, S., Kruger, R. P., Corbeil, L. B., Koller, A., Mendez, J. C., Zekarias, B., Lazar, C., and Dixon, J. E. (2009) The fic domain: regulation of cell signaling by adenylylation. *Mol. Cell* **34,** 93–103
9. Luong, P., Kinch, L. N., Brautigam, C. A., Grishin, N. V., Tomchick, D. R., and Orth, K. (2010) Kinetic and structural insights into the mechanism of AMPylation by VopS Fic domain. *J. Biol. Chem.* **285,** 20155–20163
10. Engel, P., Goepfert, A., Stanger, F. V., Harms, A., Schmidt, A., Schirmer, T., and Dehio, C. (2012) Adenylylation control by intra- or intermolecular active-site obstruction in Fic proteins. *Nature* **482,** 107–110
11. Mukherjee, S., Liu, X., Arasaki, K., McDonough, J., Galán, J. E., and Roy, C. R. (2011) Modulation of Rab GTPase function by a protein phosphocholine transferase. *Nature* **477,** 103–106
12. Campanacci, V., Mukherjee, S., Roy, C. R., and Cherfils, J. (2013) Structure of the *Legionella* effector AnkX reveals the mechanism of phosphocholine transfer by the FIC domain. *EMBO J.* **32,** 1469–1477
13. Feng, F., Yang, F., Rong, W., Wu, X., Zhang, J., Chen, S., He, C., and Zhou, J. M. (2012) A *Xanthomonas* uridine 5′-monophosphate transferase inhibits plant immune kinases. *Nature* **485,** 114–118
14. Castro-Roa, D., Garcia-Pino, A., De Gieter, S., van Nuland, N. A., Loris, R., and Zenkin, N. (2013) The Fic protein Doc uses an inverted substrate to phosphorylate and inactivate EF-Tu. *Nat. Chem. Biol.* **9,** 811–817
15. Cruz, J. W., Rothenbacher, F. P., Maehigashi, T., Lane, W. S., Dunham, C. M., and Woychik, N. A. (2014) Doc toxin is a kinase that inactivates elongation factor Tu. *J. Biol. Chem.* **289,** 7788–7798
16. Woolery, A. R., Luong, P., Broberg, C. A., and Orth, K. (2010) AMPylation: something old is new again. *Front. Microbiol.* **1,** 113
17. Itzen, A., Blankenfeldt, W., and Goody, R. S. (2011) Adenylylation: renaissance of a forgotten post-translational modification. *Trends Biochem. Sci.* **36,** 221–228
18. Rahman, M., Ham, H., Liu, X., Sugiura, Y., Orth, K., and Krämer, H. (2012) Visual neurotransmission in *Drosophila* requires expression of Fic in glial capitate projections. *Nat. Neurosci.* **15,** 871–875
19. Ham, H., Woolery, A. R., Tracy, C., Stenesen, D., Krämer, H., and Orth, K. (2014) Unfolded protein response-regulated *Drosophila* Fic (dFic) reversibly AMPylates BiP during endoplasmic reticulum homeostasis. *J. Biol. Chem.* **289,** 36059–36069
20. Goehler, H., Lalowski, M., Stelzl, U., Waelter, S., Stroedicke, M., Worm, U., Droege, A., Lindenberg, K. S., Knoblich, M., Haenig, C., Herbst, M., Suopanki, J., Scherzinger, E., Abraham, C., Bauer, B., Hasenbank, R., Fritzsche, A., Ludewig, A. H., Büssow, K., Buessow, K., Coleman, S. H., Gutekunst, C. A., Landwehrmeyer, B. G., Lehrach, H., and Wanker, E. E. (2004) A protein interaction network links GIT1, an enhancer of huntingtin aggregation, to Huntington's disease. *Mol. Cell* **15,** 853–865
21. Hao, Y. H., Chuang, T., Ball, H. L., Luong, P., Li, Y., Flores-Saaib, R. D., and Orth, K. (2011) Characterization of a rabbit polyclonal antibody against threonine-AMPylation. *J. Biotechnol.* **151,** 251–254
22. Lewallen, D. M., Sreelatha, A., Dharmarajan, V., Madoux, F., Chase, P., Griffin, P. R., Orth, K., Hodder, P., and Thompson, P. R. (2014) Inhibiting

AMPylation: a novel screen to identify the first small molecule inhibitors of protein AMPylation. *ACS Chem. Biol.* **9,** 433–442
23. Leavy, O. (2010) Therapeutic antibodies: past, present and future. *Nat. Rev. Immunol.* **10,** 297
24. Dougan, S. K., Ashour, J., Karssemeijer, R. A., Popp, M. W., Avalos, A. M., Barisa, M., Altenburg, A. F., Ingram, J. R., Cragnolini, J. J., Guo, C., Alt, F. W., Jaenisch, R., and Ploegh, H. L. (2013) Antigen-specific B-cell receptor sensitizes B cells to infection by influenza virus. *Nature* **503,** 406–409
25. Harmsen, M. M., van Solt, C. B., van Zijderveld-van Bemmel, A. M., Niewold, T. A., and van Zijderveld, F. G. (2006) Selection and optimization of proteolytically stable llama single-domain antibody fragments for oral immunotherapy. *Appl. Microbiol. Biotechnol.* **72,** 544–551
26. Kirchhofer, A., Helma, J., Schmidthals, K., Frauer, C., Cui, S., Karcher, A., Pellis, M., Muyldermans, S., Casas-Delucchi, C. S., Cardoso, M. C., Leonhardt, H., Hopfner, K. P., and Rothbauer, U. (2010) Modulation of protein properties in living cells using nanobodies. *Nat. Struct. Mol. Biol.* **17,** 133–138
27. Caussinus, E., Kanca, O., and Affolter, M. (2012) Fluorescent fusion protein knockout mediated by anti-GFP nanobody. *Nat. Struct. Mol. Biol.* **19,** 117–121
28. Rasmussen, S. G., Choi, H. J., Fung, J. J., Pardon, E., Casarosa, P., Chae, P. S., Devree, B. T., Rosenbaum, D. M., Thian, F. S., Kobilka, T. S., Schnapp, A., Konetzki, I., Sunahara, R. K., Gellman, S. H., Pautsch, A., Steyaert, J., Weis, W. I., and Kobilka, B. K. (2011) Structure of a nanobody-stabilized active state of the β_2 adrenoceptor. *Nature* **469,** 175–180
29. Wuethrich, I., Peeters, J. G., Blom, A. E., Theile, C. S., Li, Z., Spooner, E., Ploegh, H. L., and Guimaraes, C. P. (2014) Site-specific chemoenzymatic labeling of aerolysin enables the identification of new aerolysin receptors. *PLoS ONE* **9,** e109883
30. Theile, C. S., Witte, M. D., Blom, A. E., Kundrat, L., Ploegh, H. L., and Guimaraes, C. P. (2013) Site-specific N-terminal labeling of proteins using sortase-mediated reactions. *Nat. Protoc.* **8,** 1800–1807
31. Swee, L. K., Guimaraes, C. P., Sehrawat, S., Spooner, E., Barrasa, M. I., and Ploegh, H. L. (2013) Sortase-mediated modification of αDEC205 affords optimization of antigen presentation and immunization against a set of viral epitopes. *Proc. Natl. Acad. Sci. U.S.A.* **110,** 1428–1433
32. Meerbrey, K. L., Hu, G., Kessler, J. D., Roarty, K., Li, M. Z., Fang, J. E., Herschkowitz, J. I., Burrows, A. E., Ciccia, A., Sun, T., Schmitt, E. M., Bernardi, R. J., Fu, X., Bland, C. S., Cooper, T. A., Schiff, R., Rosen, J. M., Westbrook, T. F., and Elledge, S. J. (2011) The pINDUCER lentiviral toolkit for inducible RNA interference *in vitro* and *in vivo*. *Proc. Natl. Acad. Sci. U.S.A.* **108,** 3665–3670
33. Sosa, B. A., Demircioglu, F. E., Chen, J. Z., Ingram, J., Ploegh, H. L., and Schwartz, T. U. (2014) How lamina-associated polypeptide 1 (LAP1) activates Torsin. *eLife* **3,** e03239
34. Schindelin, J., Arganda-Carreras, I., Frise, E., Kaynig, V., Longair, M., Pietzsch, T., Preibisch, S., Rueden, C., Saalfeld, S., Schmid, B., Tinevez, J. Y., White, D. J., Hartenstein, V., Eliceiri, K., Tomancak, P., and Cardona, A. (2012) Fiji: an open-source platform for biological-image analysis. *Nat. Methods* **9,** 676–682
35. Mukherjee, J., Tremblay, J. M., Leysath, C. E., Ofori, K., Baldwin, K., Feng, X., Bedenice, D., Webb, R. P., Wright, P. M., Smith, L. A., Tzipori, S., and Shoemaker, C. B. (2012) A novel strategy for development of recombinant antitoxin therapeutics tested in a mouse botulism model. *PLoS ONE* **7,** e29941
36. Bailey, T. L., Boden, M., Buske, F. A., Frith, M., Grant, C. E., Clementi, L., Ren, J., Li, W. W., and Noble, W. S. (2009) MEME SUITE: tools for motif discovery and searching. *Nucleic Acids Res.* **37,** W202–W208
37. Sundberg, E. J., and Mariuzza, R. A. (2002) Molecular recognition in antibody-antigen complexes. *Adv. Protein Chem.* **61,** 119–160
38. Mishra, N., Buelens, K., Theyskens, S., Compernolle, G., Gils, A., and Declerck, P. J. (2012) Increased zymogen activity of thrombin-activatable fibrinolysis inhibitor prolongs clot lysis. *J. Thromb. Haemost.* **10,** 1091–1099
39. Bunney, T. D., Cole, A. R., Broncel, M., Esposito, D., Tate, E. W., and Katan, M. (2014) Crystal structure of the human, FIC-domain containing protein HYPE and implications for its functions. *Structure* 10.1016/j.str.2014.10.007
40. Sanyal, A., Chen, A. J., Nakayasu, E. S., Lazar, C. S., Zbornik, E. A., Worby, C. A., Koller, A., and Mattoo, S. (2015) A novel link between Fic (filamentation induced by cAMP)-mediated adenylylation/AMPylation and the unfolded protein response. *J. Biol. Chem.* 10.1074/jbc.M114.618348
41. González, J. M., and Andrés, V. (2011) Synthesis, transport and incorporation into the nuclear envelope of A-type lamins and inner nuclear membrane proteins. *Biochem. Soc. Trans.* **39,** 1758–1763
42. Coffinier, C., Jung, H. J., Li, Z., Nobumori, C., Yun, U. J., Farber, E. A., Davies, B. S., Weinstein, M. M., Yang, S. H., Lammerding, J., Farahani, J. N., Bentolila, L. A., Fong, L. G., and Young, S. G. (2010) Direct synthesis of lamin A, bypassing prelamin a processing, causes misshapen nuclei in fibroblasts but no detectable pathology in mice. *J. Biol. Chem.* **285,** 20818–20826
43. Burzio, L. O., Riquelme, P. T., and Koide, S. S. (1979) ADP-ribosylation of rat liver nucleosomal core histones. *J. Biol. Chem.* **254,** 3029–3037
44. Boulikas, T. (1989) DNA strand breaks alter histone ADP-ribosylation. *Proc. Natl. Acad. Sci. U.S.A.* **86,** 3499–3503
45. Shimada, M., Niida, H., Zineldeen, D. H., Tagami, H., Tanaka, M., Saito, H., and Nakanishi, M. (2008) Chk1 is a histone H3 threonine 11 kinase that regulates DNA damage-induced transcriptional repression. *Cell* **132,** 221–232
46. Lin, S., and Garcia, B. A. (2012) Examining histone posttranslational modification patterns by high-resolution mass spectrometry. *Methods Enzymol.* **512,** 3–28